Supplementary Materials for

Climate change and human activities amplify runoff variability risks in lower reaches of large rivers

Ju Gao[1,2], Chunhui Li[1,2,*], Xiong Zhou[1*], Yujun Yi[1], Xuan Wang[1,2], and Qiang Liu[1,2]

[1] Key Lab of Water and Sediment Science of Ministry of Education, School of Environment, Beijing Normal University, Beijing, China

[2] State Key Laboratory of Wetland Conservation and Restoration, School of Environment, Beijing Normal University, Beijing, China

* Corresponding author at: chunhuili@bnu.edu.cn, zhou.xiong@outlook.com

This file includes:

Supplementary Methods: five commonly used change point detection methods.

Supplementary Figures: 1 to 18

Supplementary Tables: 1 to 5

Supplementary Methods

Change point detection methods

We employ five widely used hydro-meteorological change point detection methods[1], including the Mann-Kendall change point detection, moving T-test change point detection, rank sum change point detection, cumulative anomaly and ordered clustering change point detection, to identify significant change points in climatic factors and hydrological station flows within each sub-catchment[2,3,4]. The purpose of using multiple change detection methods is to increase the confidence of the detection results. The specific steps of each change point detection method are as follows.

the Mann-Kendall change point detection:

The Mann-Kendall change point detection is a non-parametric method for detecting abrupt changes. For a time series $X = \{x_1, x_2, \cdots, x_n\}$ with length n, the first step is to perform a rank transformation, constructing an order column:

$$S_k = \sum_{i=1}^{k} R_i \ \ (k = 2, 3, \cdots, n) \tag{1}$$

$$R_i = \begin{cases} 1; & x_i > x_j \\ 0; & x_i \leq x_j \end{cases} \quad (k = 1, 2, \cdots, n) \tag{2}$$

The order column S_k is the cumulative number of instances where the value at moment i is greater than that at moment j. Under the assumption of random independence in the time series, the Mann-Kendall test statistic can be defined as follows:

$$UF_k = \frac{[S_k - E(S_k)]}{\sqrt{Var(S_k)}} \quad (k = 1,2, \cdots, n) \tag{3}$$

$$E(S_k) = \frac{n(n+1)}{4} \tag{4}$$

$$Var(S_k) = \frac{n(n-1)(2n+5)}{72} \tag{5}$$

Reverse the order of the time series and repeat the above steps to calculate:

$$UB_k = -\frac{[S'_k - E'(S'_k)]}{\sqrt{Var(S'_k)}} \quad (k = 1,2, \cdots, n) \tag{6}$$

Among them, S'_k, $E'(S'_k)$, and $Var(S'_k)$ are respectively the cumulative number, mean value, and variance of the order column after the time series is reversed. Plot the UF_k and UB_k curves. If the value of UF_k or UB_k is greater than 0, it indicates that the sequence shows an upward trend; if less than 0, it indicates a downward trend. When they exceed the critical line, it signifies a significant upward or downward trend. The range where they exceed the critical line is determined as the time period during which an abrupt change occurs. If the two curves intersect and the intersection point is between the critical lines, then the moment corresponding to the intersection point is the start time of the abrupt change.

Moving T-test change point detection：

The moving T-test change point detection examines whether there is a significant difference between the means of two sub-sequences in a hydrological and climatic sequence by treating it as a problem of determining whether there is a significant difference between the means of two populations. Here are the formula and method for the moving T-test:

$$T = \frac{\bar{x}_1 - \bar{x}_2}{\sqrt{\frac{S_1^2}{n_1} + \frac{S_2^2}{n_2}}} \tag{7}$$

$$\bar{x}_1 = \frac{1}{n_1}\sum_{i=1}^{n_1} x_i \tag{8}$$

$$\bar{x}_2 = \frac{1}{n_2}\sum_{j=1}^{n_2} x_j \tag{9}$$

$$S_1^2 = \frac{1}{n_1 - 1}\sum_{i=1}^{n_1}(x_i - \bar{x}_1)^2 \tag{10}$$

$$S_2^2 = \frac{1}{n_2 - 1}\sum_{j=1}^{n_2}\left(x_j - \bar{x}_2\right)^2 \tag{11}$$

where T is the test statistic, which follows a t-distribution with $n_1 + n_2 - 2$ degree of freedom. n_1, x_i, and S_1^2 are respectively the length, the i-th data point, and the variance of the first subsequence. n_2, x_j, and S_2^2 are respectively the length, the i-th data point, and the variance of the second subsequence. Compare the calculated T

value with the critical value of the t-distribution corresponding to the given significance level. If T is greater than the critical value, it is considered that there is an abrupt change at that position.

Rank sum change point detection:

By conducting a point-by-point examination of the sequence through the sliding rank sum test method, it is possible to effectively identify the change points in the series data. The following is the formula and method for the sliding rank sum change point detection.

For time series $X = \{x_1, x_2, \cdots, x_n\}$, determine an appropriate window size w based on the specific application scenario and data characteristics. Let R_i be the sum of ranks in the i-th window, $R_{(i,1)}$ be the sum of ranks at the start position of the window, and $R_{(i,2)}$ be the sum of ranks at the end position of the window. $E(R_i)$ is the expected value of R_i, and $Var(R_i)$ is the variance of R_i. The statistic Z_i is then given by:

$$Z_i = \frac{R_i - E(R_i)}{\sqrt{Var(R_i)}} \tag{12}$$

$$E(R_i) = \frac{w(w+1)(2w+1)}{6} \tag{13}$$

$$Var(R_i) = \frac{w(w+1)(2w+1)}{18} \tag{14}$$

If the absolute value of the statistic Z_i exceeds a predetermined critical value, there may be a change point. Based on the positions of $R_{(i,1)}$ and $R_{(i,2)}$, find the corresponding original sequence positions, which are the locations of the change points.

Cumulative anomaly:

Given a time series $X = \{x_1, x_2, \cdots, x_n\}$, the formula for calculating the average value $\bar{x}$ is:

$$\bar{x} = \frac{1}{n}\sum_{i=1}^{n} x_i \tag{15}$$

For each data point x_i, the formula for calculating the anomaly d_i is:

$$d_i = x_i - \bar{x} \tag{16}$$

The formula for calculating the cumulative anomaly D_i is:

$$D_i = \sum_{j=1}^{i} d_j = \sum_{j=1}^{i} (x_j - \bar{x}) \quad (i = 1,2,\cdots,n) \tag{17}$$

By plotting the cumulative anomaly values as a curve graph, it is possible to visually observe the long-term trend over time. The inclination of the curve, inflection points, and the amplitude and period of fluctuations can all reflect the changing characteristics of the variable and its underlying potential causes.

Ordered clustering change point detection:

The ordered clustering change point test method seeks the optimal segmentation point by minimizing the sum of squared deviations within each class. Given a time series $X = \{x_1, x_2, \cdots, x_n\}$, if we assume that the possible change point is r, then the sum of squared deviations before and after the change point are given by:

$$S_1 = \sum_{i=1}^{r} (x_i - \bar{x}_1)^2 \tag{18}$$

$$S_2 = \sum_{i=r+1}^{n} (x_i - \bar{x}_2)^2 \tag{19}$$

$$\bar{x}_1 = \frac{1}{r} \sum_{i=1}^{r} x_i \tag{20}$$

$$\bar{x}_2 = \frac{1}{n-r} \sum_{i=r+1}^{n} x_i \tag{21}$$

where $\bar{x}_1$ and $\bar{x}_2$ are the means of the sequences before and after the mutation point r, respectively, which are also the cluster centers of the two sequences.

Thus, the objective function to be minimized is:

$$S = \min_{2 \leq r \leq n-1} (S_1 + S_2) \tag{22}$$

where 'min' denotes the minimum value. When S takes the minimum value, the corresponding r is the optimal bisection point, which can be inferred as the mutation point.

Supplementary Figures

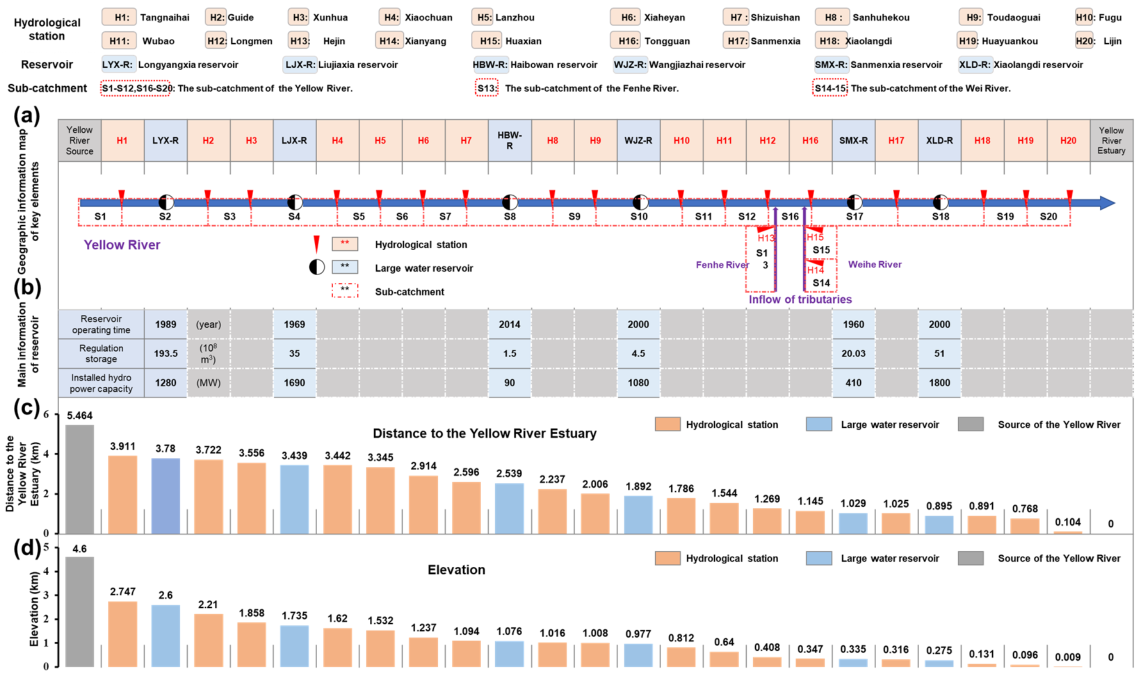

Supplementary Fig. 1: Basic information on hydrological stations, large reservoirs, and sub-catchments in the Yellow River basin. (a):** Simplified diagram of the relative positions between hydrological stations, large reservoirs, and sub-catchments. **(b):** Basic information on the operation time, regulating capacity, and power generation of each reservoir. The distances from the main stream's hydrological stations and large reservoirs to the estuary of the Yellow River **(c)** and their elevations **(d).**

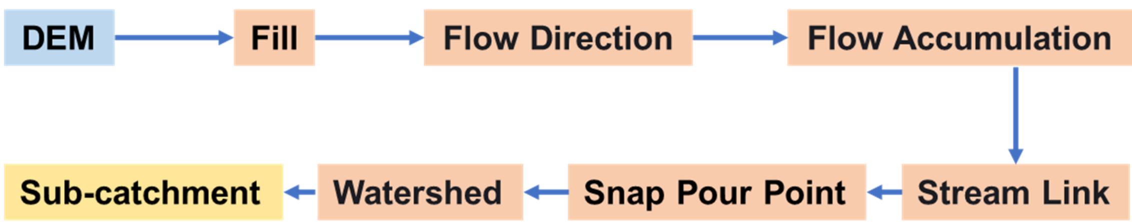

Supplementary Fig. 2: Hydrological analysis steps for sub-catchment delineation based on ArcGIS 10.3 software. Set the parallel processing factor in the environmental settings of each hydrological analysis tool to 0.

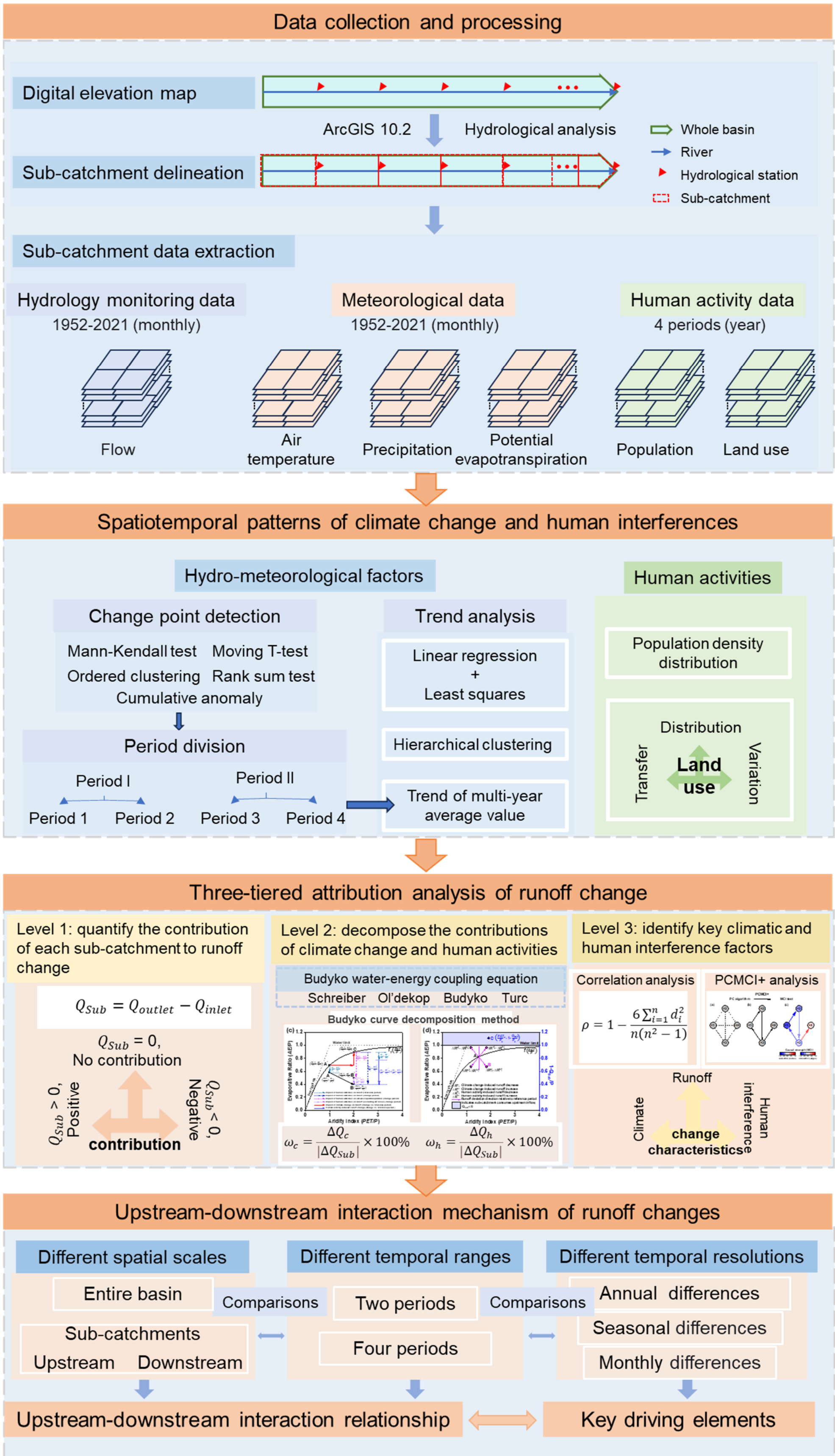

Supplementary Fig. 3: The overall framework of the research process and the three-tiered attribution analysis method for streamflow variation.

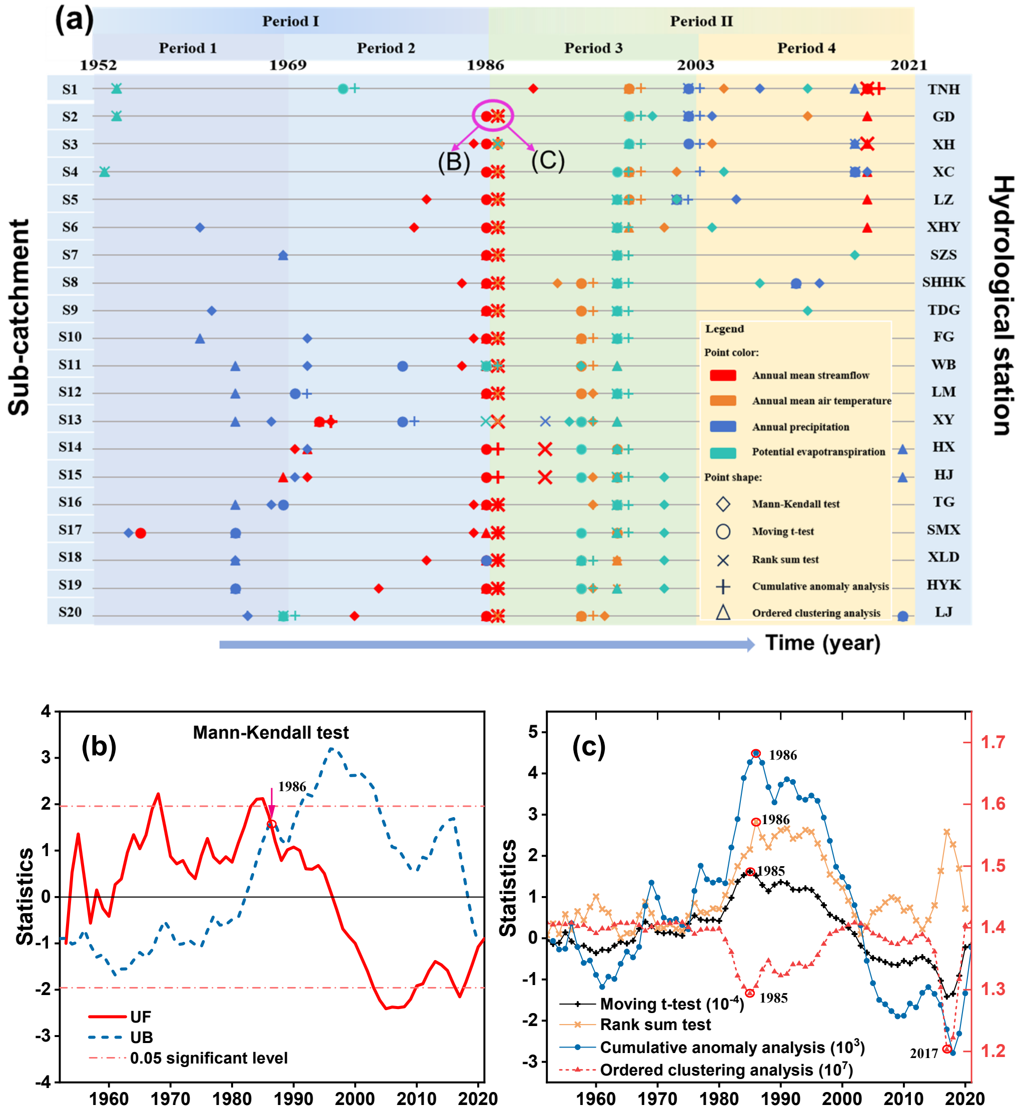

Supplementary Fig. 4: The abrupt change points of the flow of each hydrological station and the air temperature, precipitation and potential evapotranspiration of each sub-catchment area in the Yellow River Basin, as well as the two-stage and four-stage change periods based on the abrupt points. (a): The abrupt change points in flow, air temperature, precipitation, and potential evapotranspiration detected based on the Mann-Kendall test, moving T-test, rank sum test, cumulative anomaly, and ordered clustering methods. The shape of the points represents different change point detection methods. The color of the points represents the flow at hydrological stations and the temperature, precipitation, and potential evapotranspiration of each sub-catchment area. The background color represents the time ranges of the different periods identified. Examples of flow change point detection at the Guide hydrological station based on the Mann-Kendall test method **(b)**, as well as the moving T-test, rank sum test, cumulative anomaly, and ordered clustering methods **(c)**.

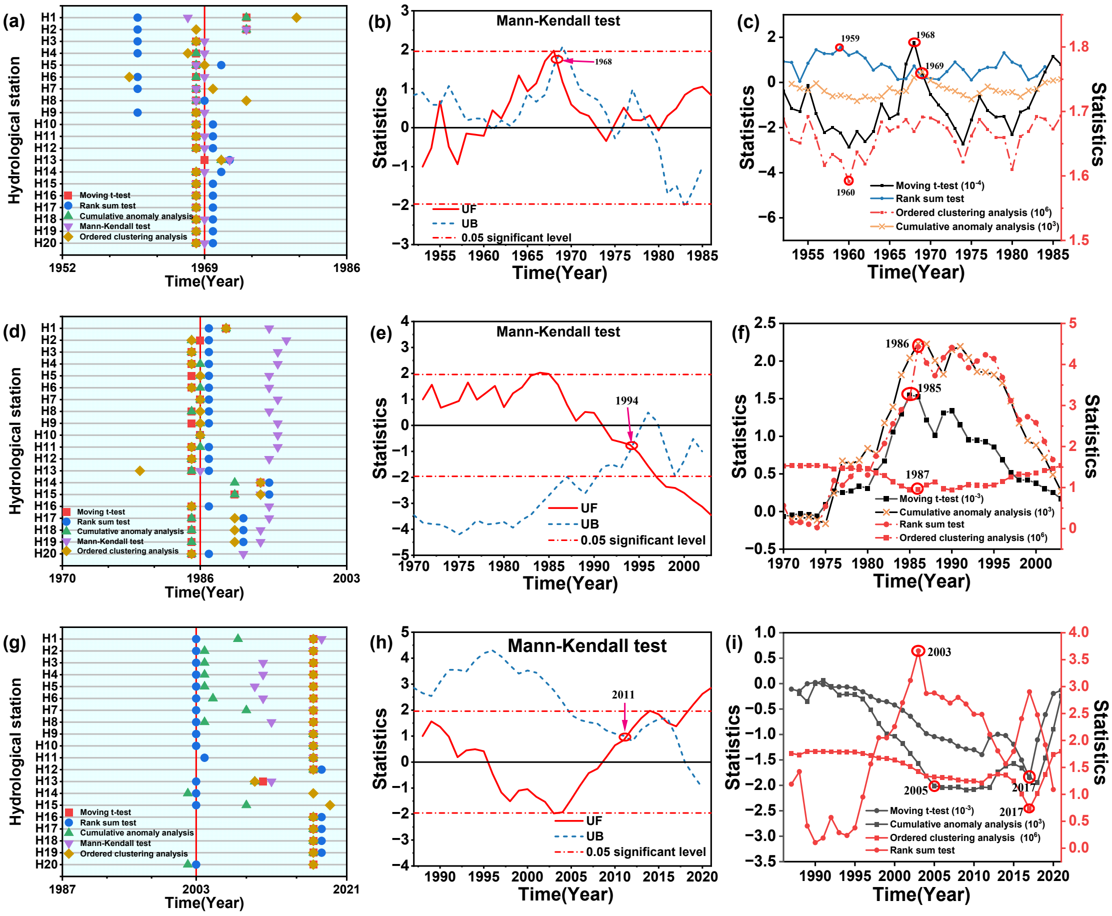

Supplementary Fig. 5: The abrupt change points of the streamflow of each hydrological station across various periods. (a), **(d)**, and **(g)** display the streamflow change points detected during 1952-1986, 1970-2003, and 1987-2021 respectively, using the Mann-Kendall change point detection, moving t-test change point detection, rank-sum change point detection, cumulative anomaly, and ordered clustering methods. The point shapes and colors represent different change point detection methods. **(b)**, **(e)**, and **(h)** illustrate examples of streamflow change point detection at XHY station using the Mann-Kendall method for 1952-1986, 1970-2003, and 1987-2021 periods respectively. Similarly, **(c)**, **(f)**, and **(i)** present the corresponding results obtained from the moving t-test change point detection, rank-sum change point detection, cumulative anomaly, and ordered clustering methods for these three periods at XHY station.

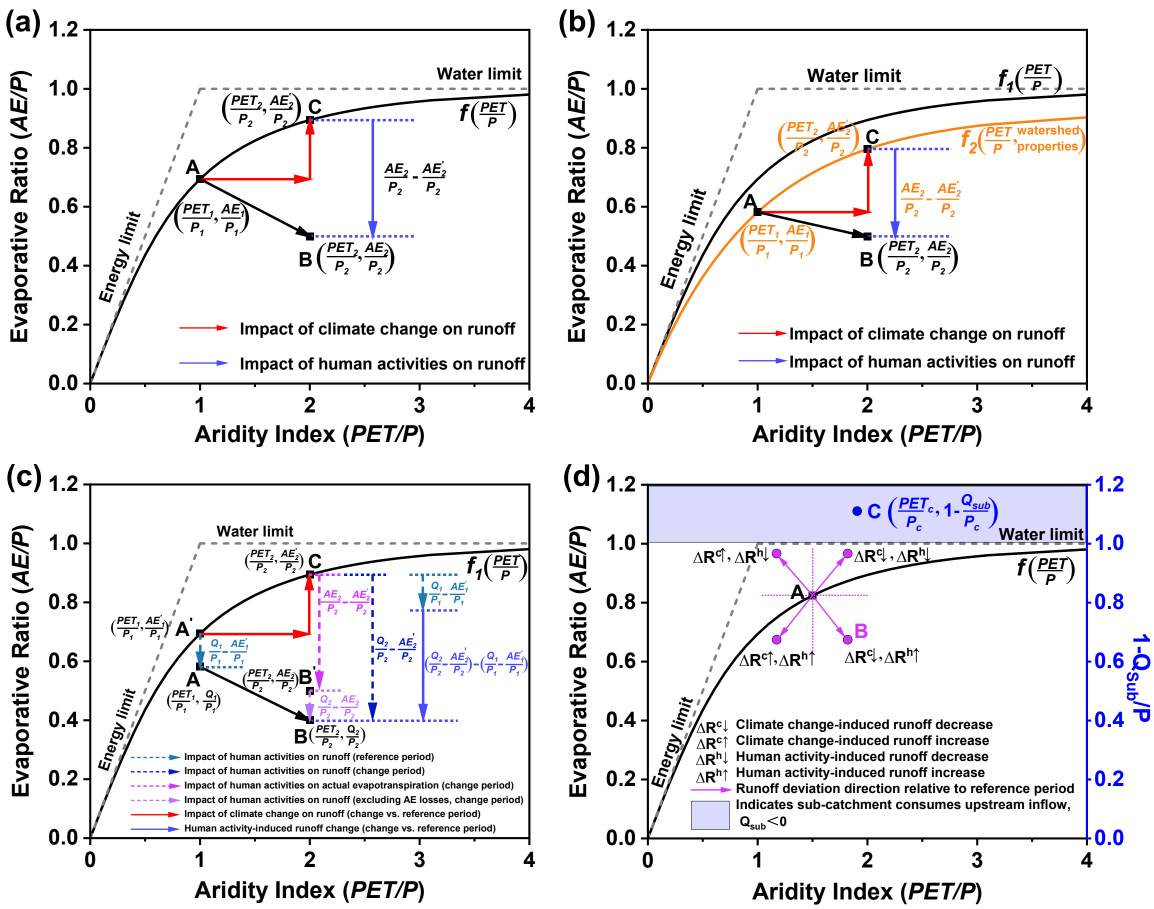

Supplementary Fig. 6: Overview of methods for decomposing the Budyko water-energy balance curve to quantify the impacts of climate change and human activities on runoff variation. **(a)** Traditional non-parametric Budyko curve decomposition method; **(b)** Parametric water-energy balance curve decomposition method; **(c)** The non-parametric Budyko curve decomposition method comparing change periods to reference periods in this study, which incorporates the impact of external water resource contributions (excluding evapotranspiration losses caused by human activities) on runoff changes; **(d)** Characteristics of climate change and human activity impacts on runoff coefficient ($\boldsymbol{R = Q_{Sub}/P}$), with anomalous zones (light blue areas) showing long-term runoff contribution amounts and precipitation relationships in midstream/downstream sub-catchments receiving external water resources.

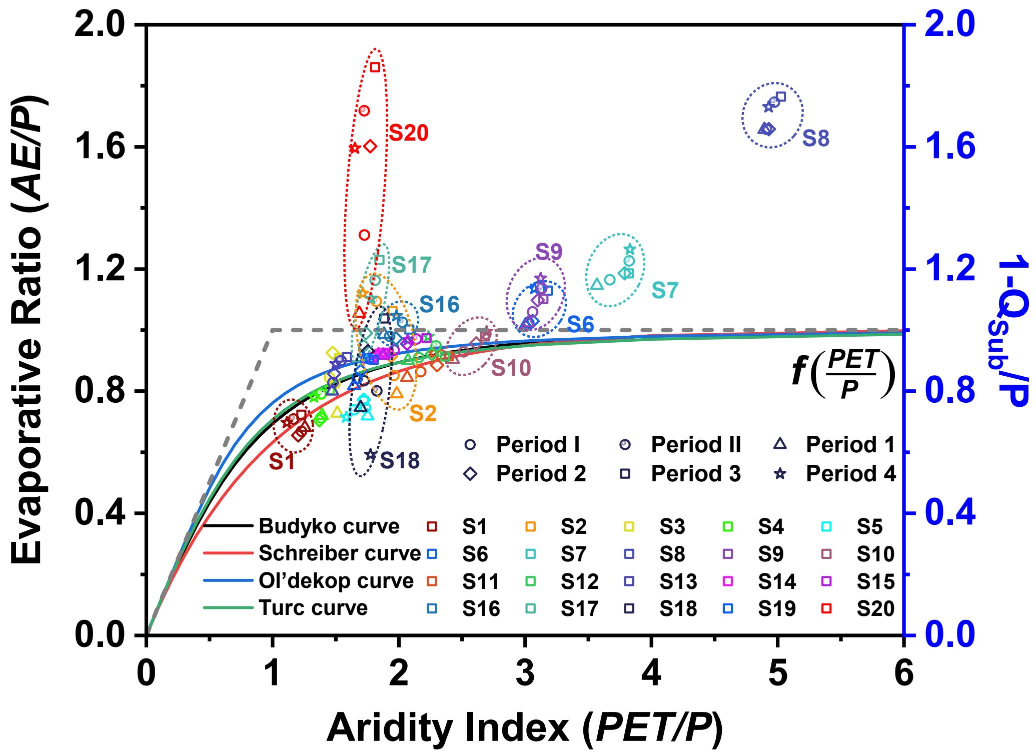

Supplementary Fig. 7: The long-term mean annual runoff contribution and precipitation relationship data for each studied sub-catchment within the Budyko water-energy balance framework. Point shapes represent different periods, while colors denote different sub-catchments. Points within the light blue zone indicate sub-catchments with negative runoff contributions to the main river, representing either severe water scarcity or reservoir construction in these sub-catchments that utilize or store exogenous water resources from upstream areas.

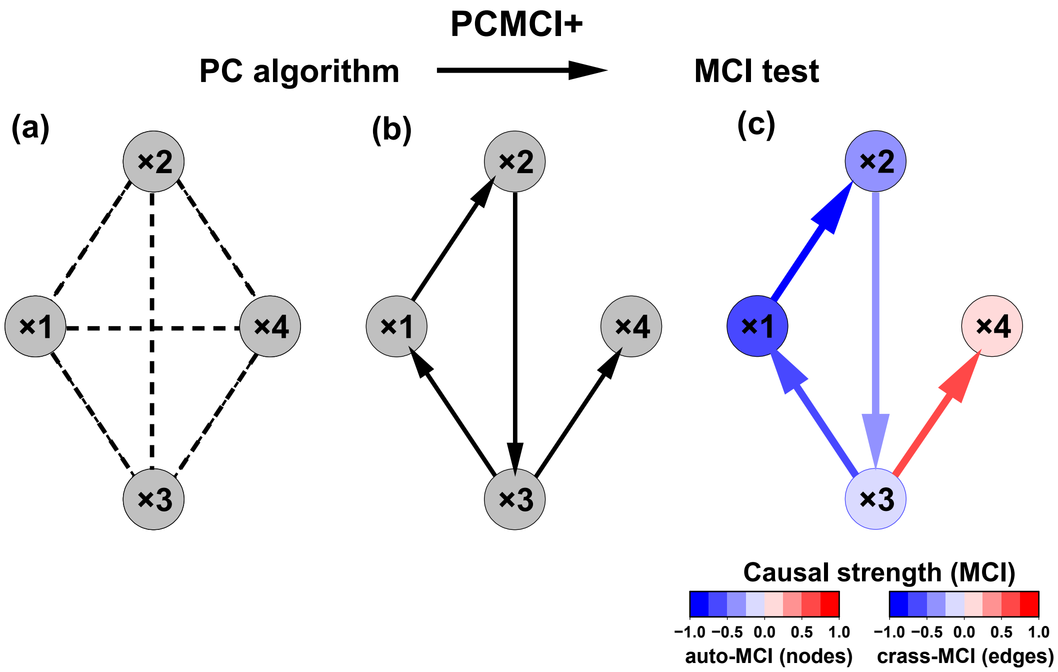

Supplementary Fig. 8: Overview of the Peter-Clark Momentary Conditional Independence Plus (PCMCI+) causal discovery algorithm. The method consists of two main steps: the PC1 algorithm and MCI tests. PC1 begins with a fully connected graph as shown in **(a)**. It then iteratively eliminates links between variables by testing conditional independence with progressively increasing conditioning sets, as illustrated in **(b)**. Finally, the MCI tests employ the estimated conditions identified in the first step to infer causal relationships **(c)**. Node colors represent the auto-dependence degree of each component (auto-MCI), while link colors indicate the mutual dependence strength between variables (cross-MCI).

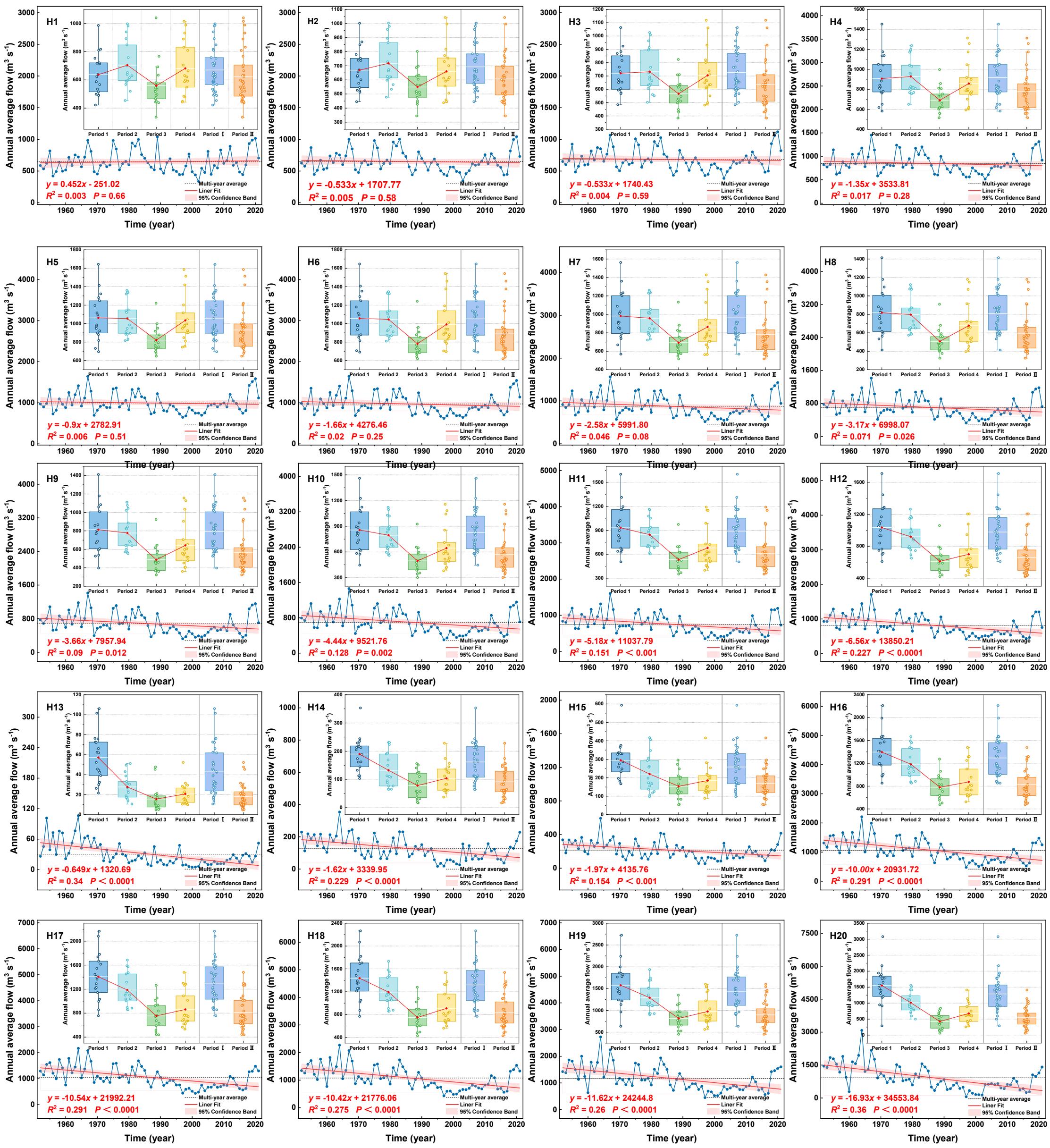

Supplementary Fig. 9: The annual variation trend of flow volumes at hydrological stations from 1952 to 2021, as well as the multi-year average changes during different periods.

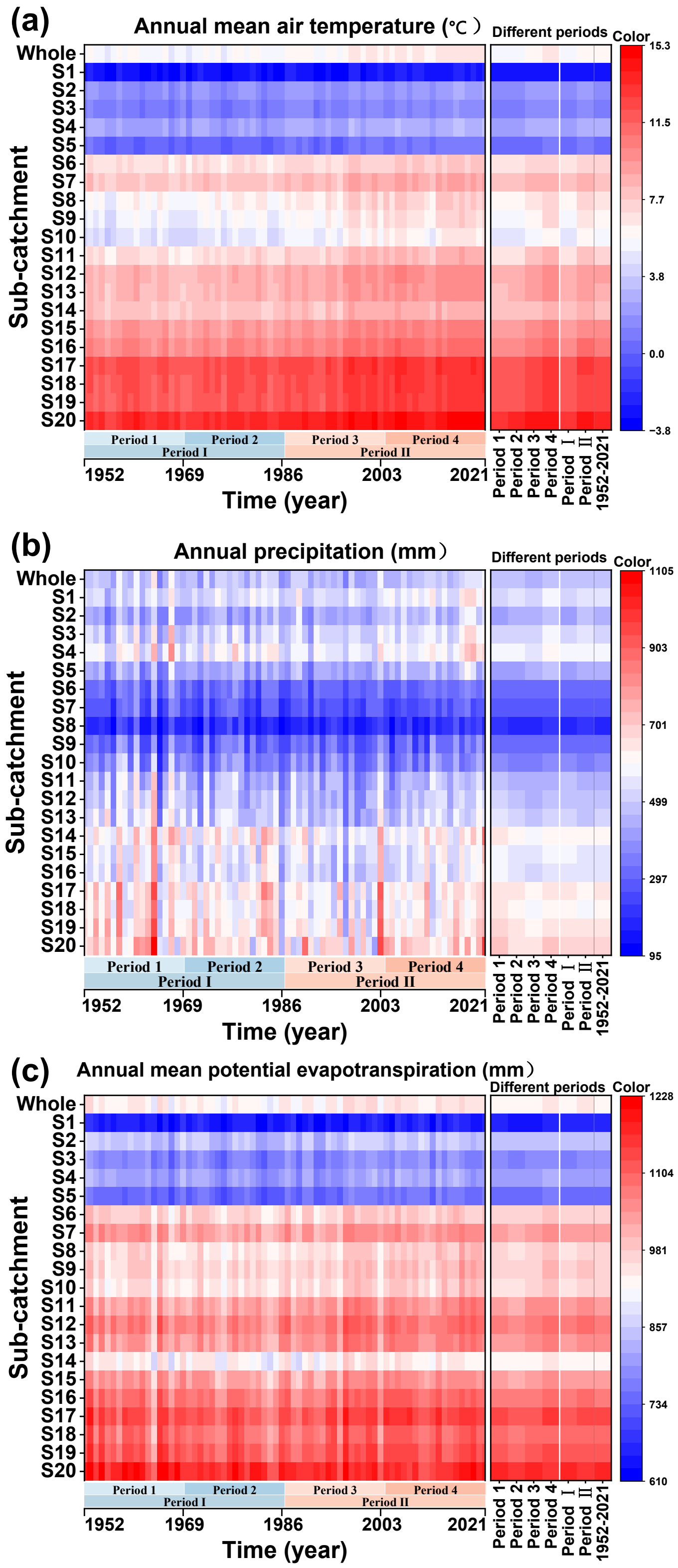

Supplementary Fig. 10: The spatiotemporal distribution characteristics of air temperature, precipitation, and potential evapotranspiration in the Yellow River Basin, as well as the differences in average values over different periods. (a): Air temperature. **(b):** Precipitation. **(c):** Potential evapotranspiration.

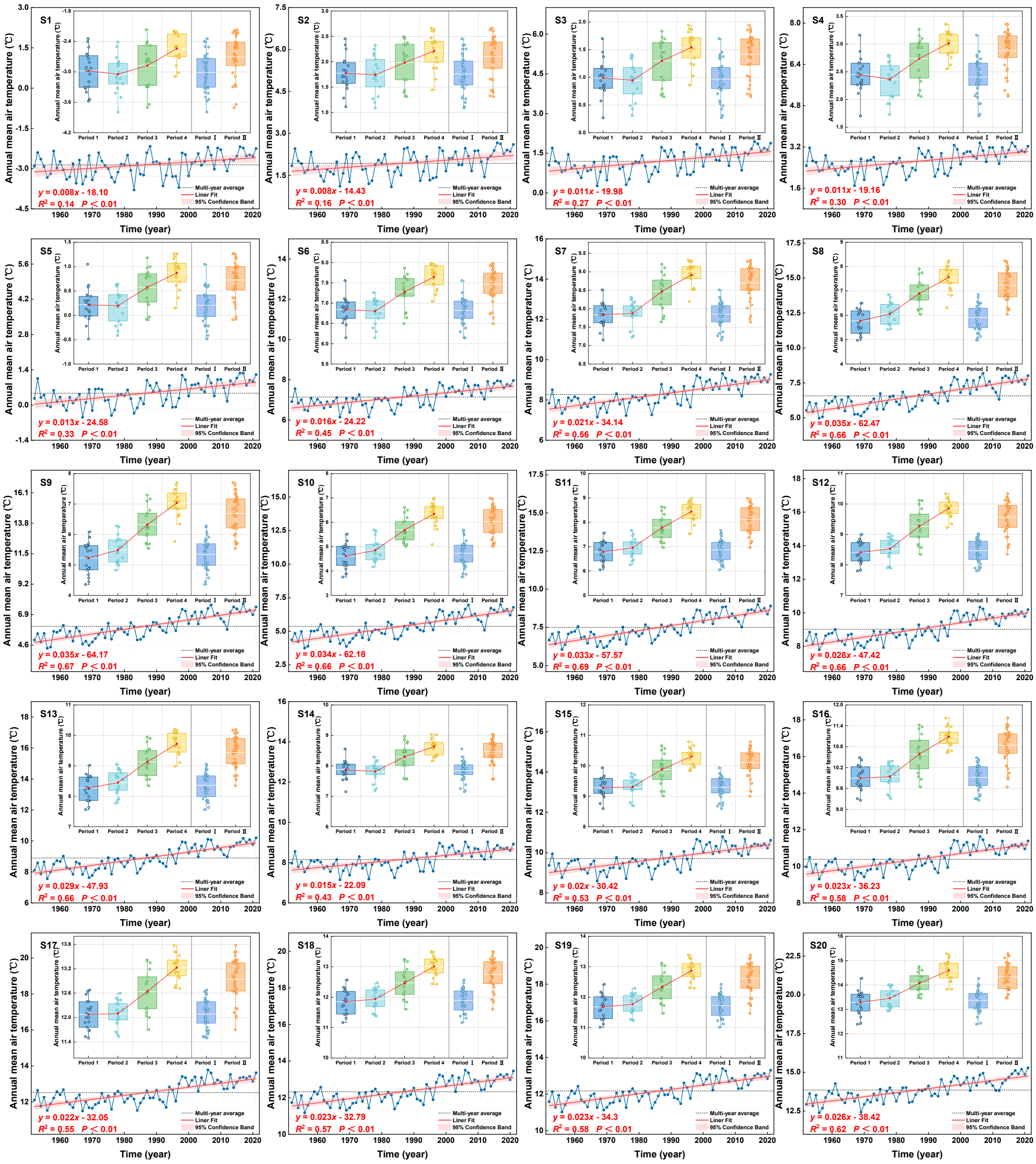

Supplementary Fig. 11: The annual variation trend of air temperature in each sub-catchment from 1952 to 2021, as well as the multi-year average changes during different periods.

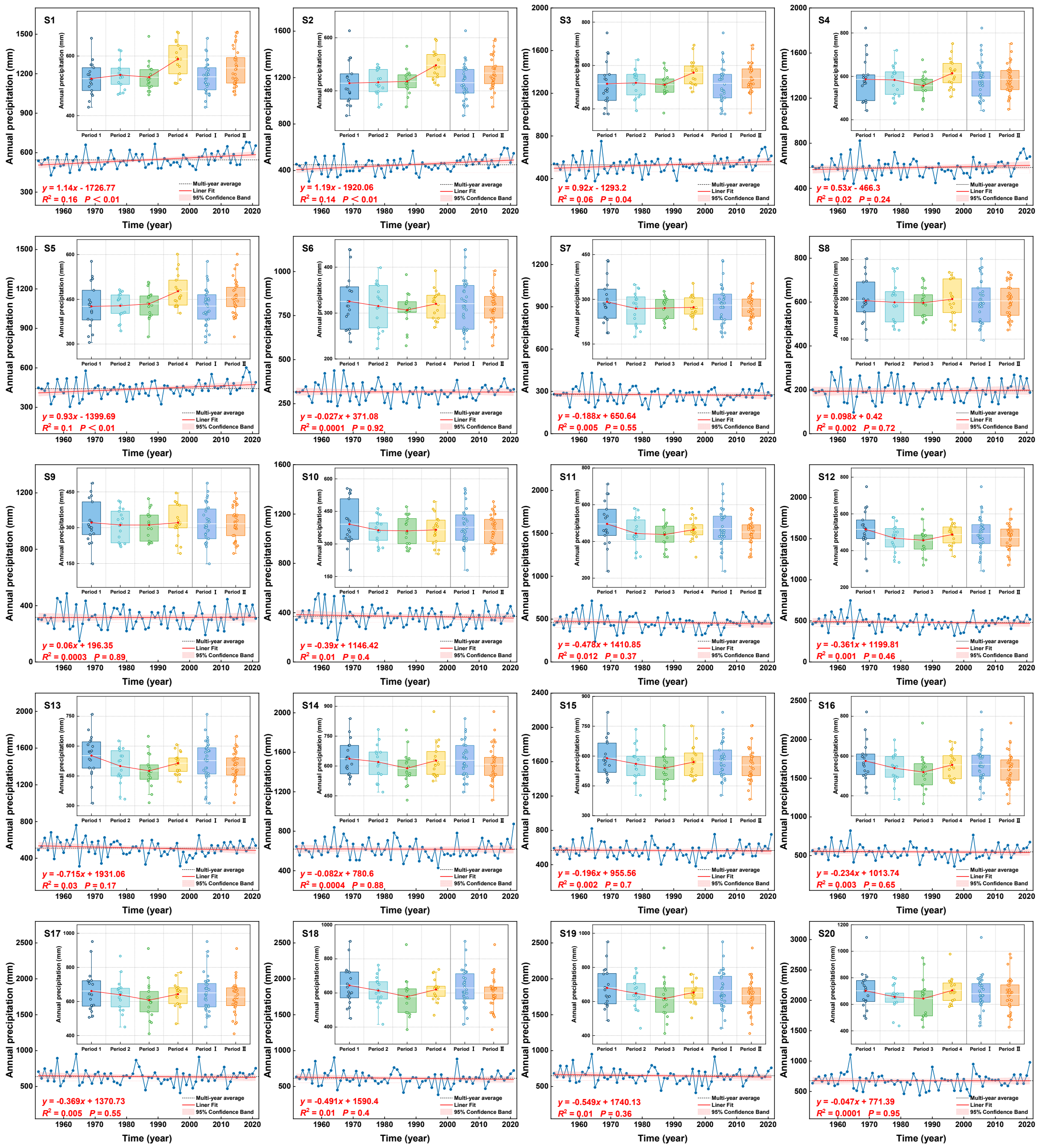

Supplementary Fig. 12: The annual variation trend of precipitation in each sub-catchment from 1952 to 2021, as well as the multi-year average changes during different periods.

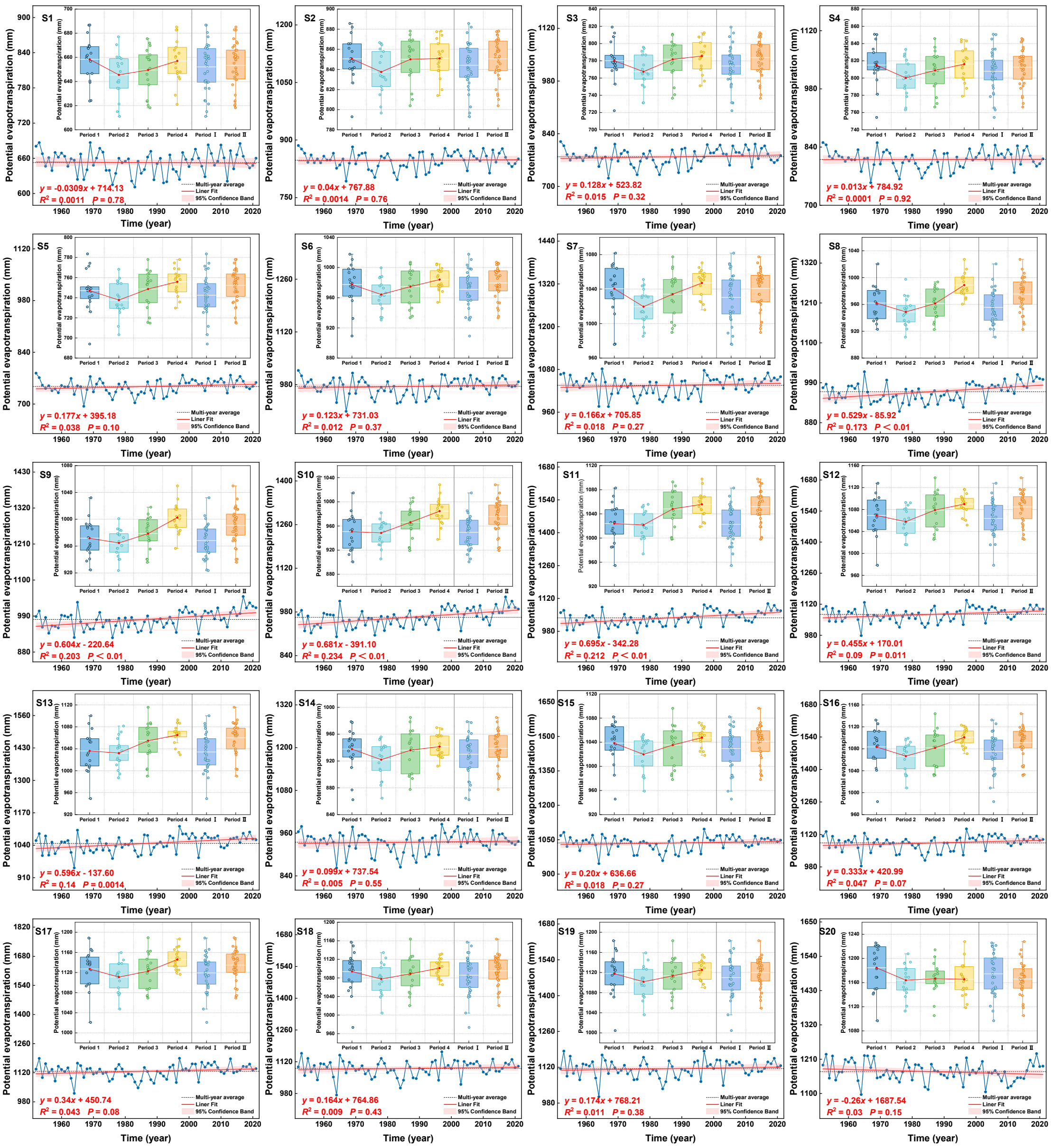

Supplementary Fig. 13: The annual variation trend of potential evapotranspiration in each sub-catchment from 1952 to 2021, as well as the multi-year average changes during different periods.

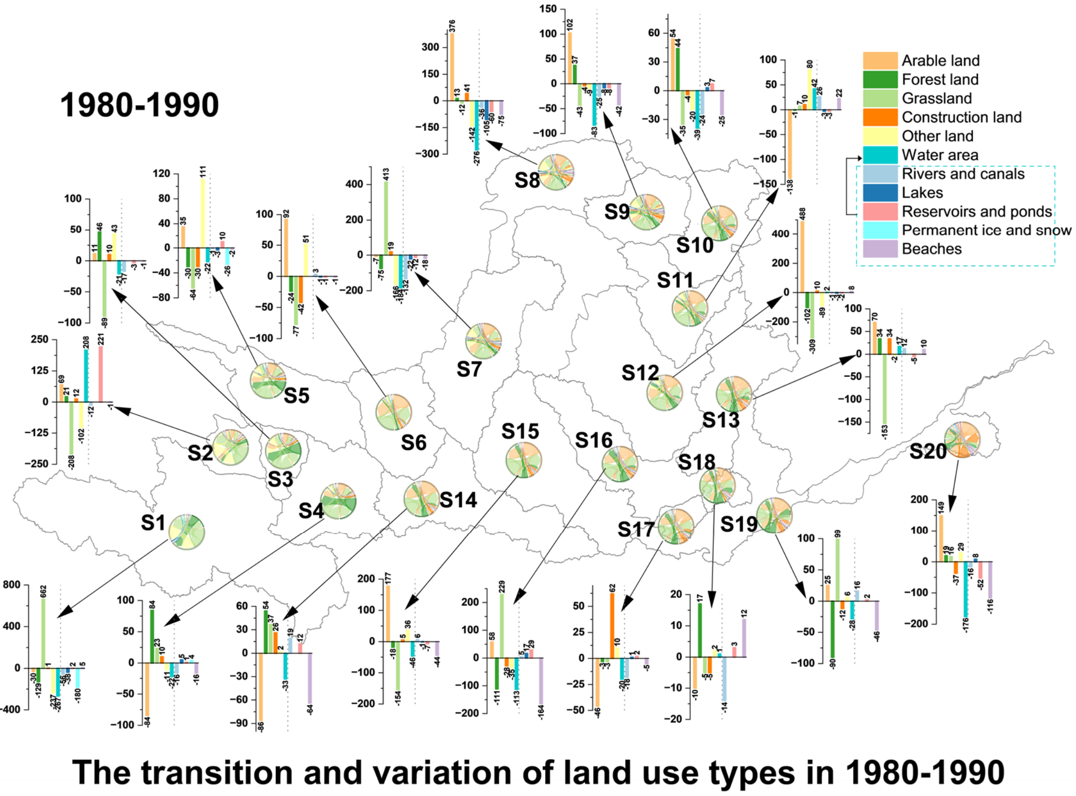

Supplementary Fig. 14: The transfer volumes and changes of various land use types in each sub-catchment from 1980 to 1990. The chord diagram represents the transfer volumes of each land use type, while the bar chart shows the change volumes of each land use type.

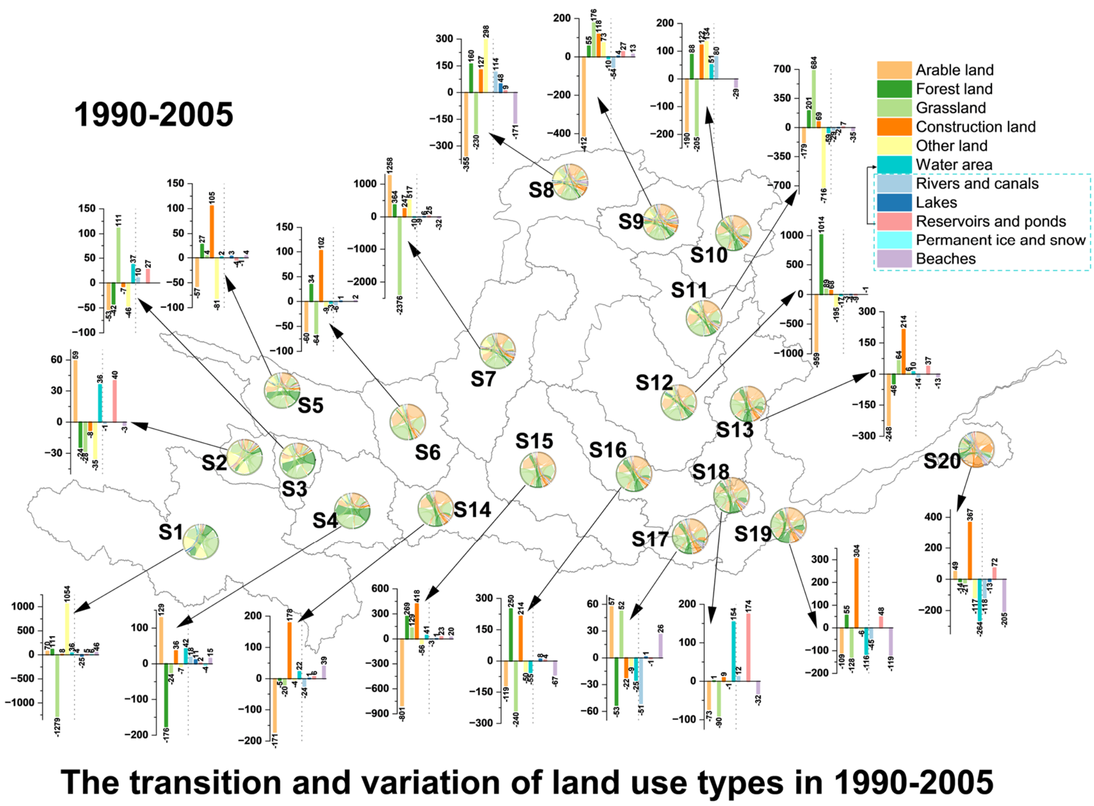

Supplementary Fig. 15: The transfer volumes and changes of various land use types in each sub-catchment from 1990 to 2005. The chord diagram represents the transfer volumes of each land use type, while the bar chart shows the change volumes of each land use type.

233

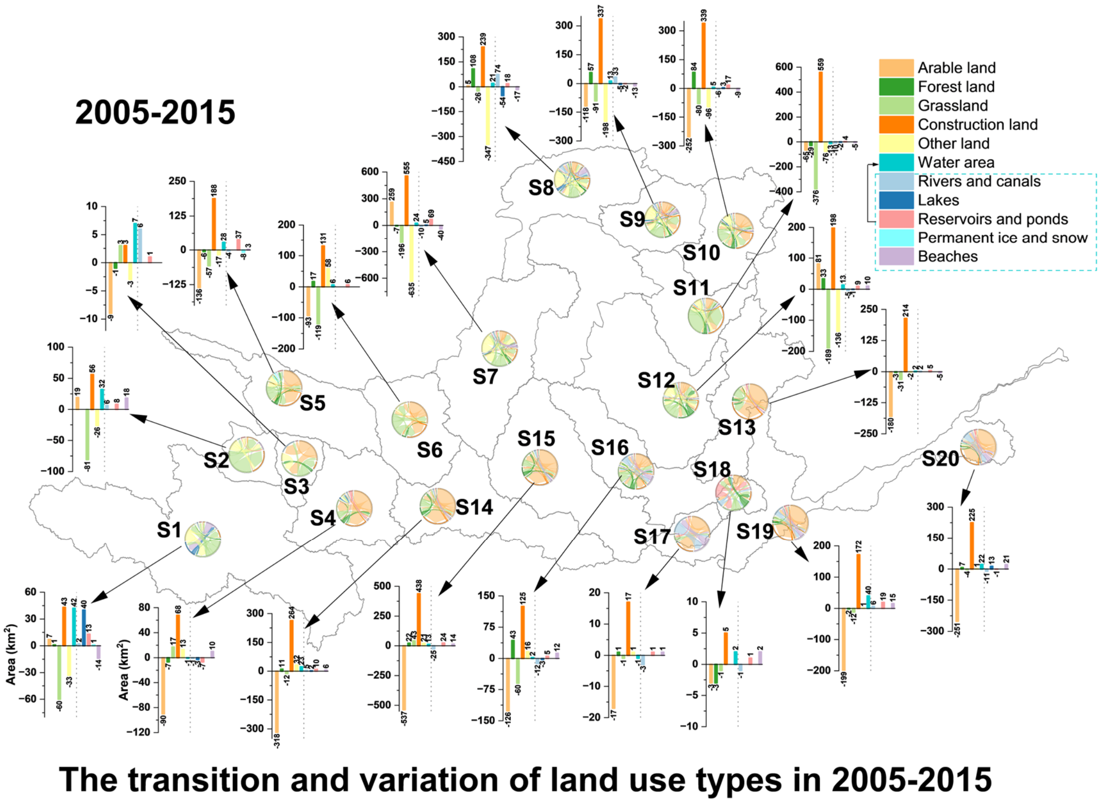

234

235 **Supplementary Fig. 16: The transfer volumes and changes of various land use**
236 **types in each sub-catchment from 2005 to 2015.** The chord diagram represents the
237 transfer volumes of each land use type, while the bar chart shows the change volumes
238 of each land use type.

239

240

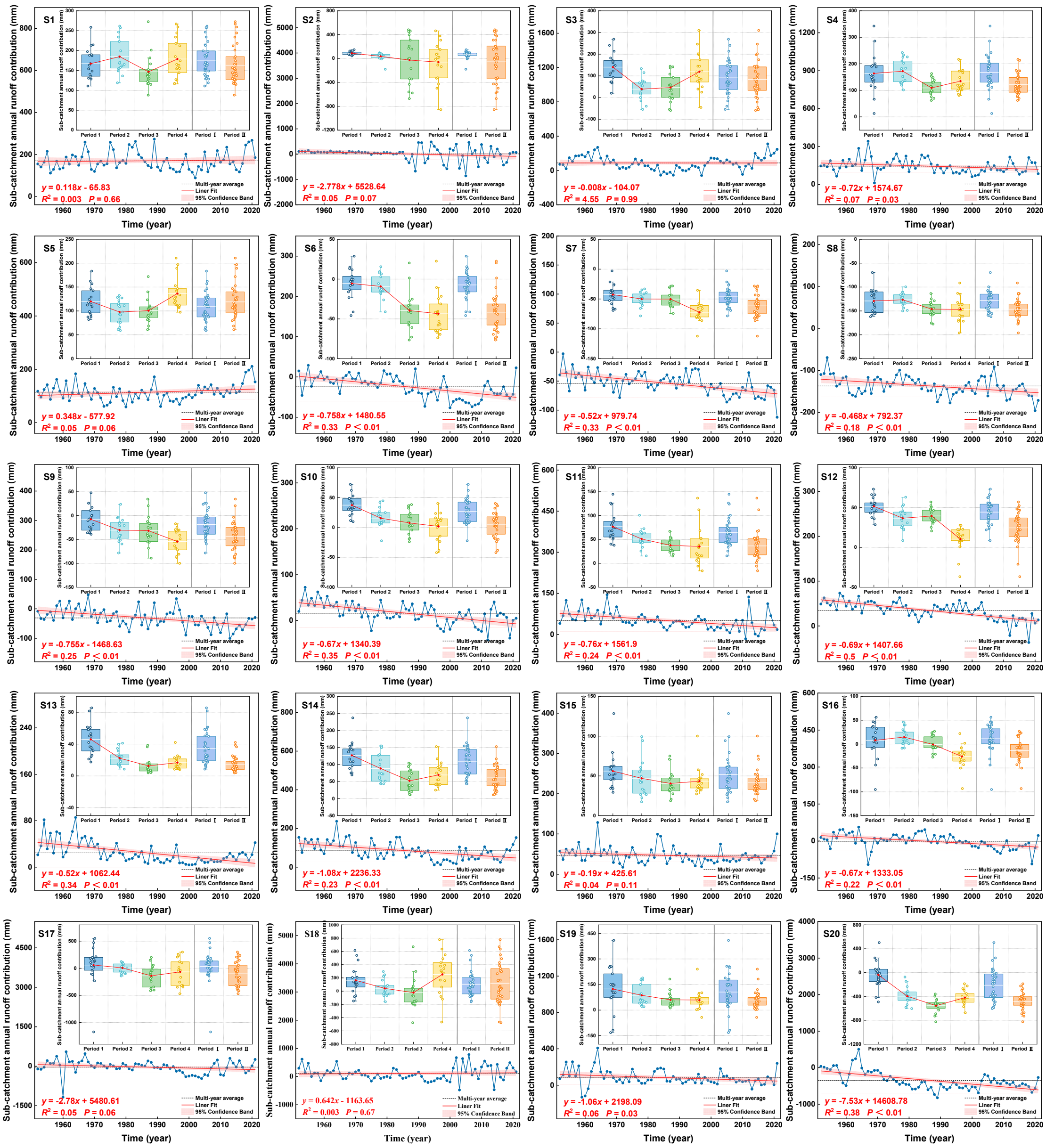

Supplementary Fig. 17: The annual variation trend of runoff contribution volumes in each sub-catchment from 1952 to 2021, as well as the multi-year average changes during different periods.

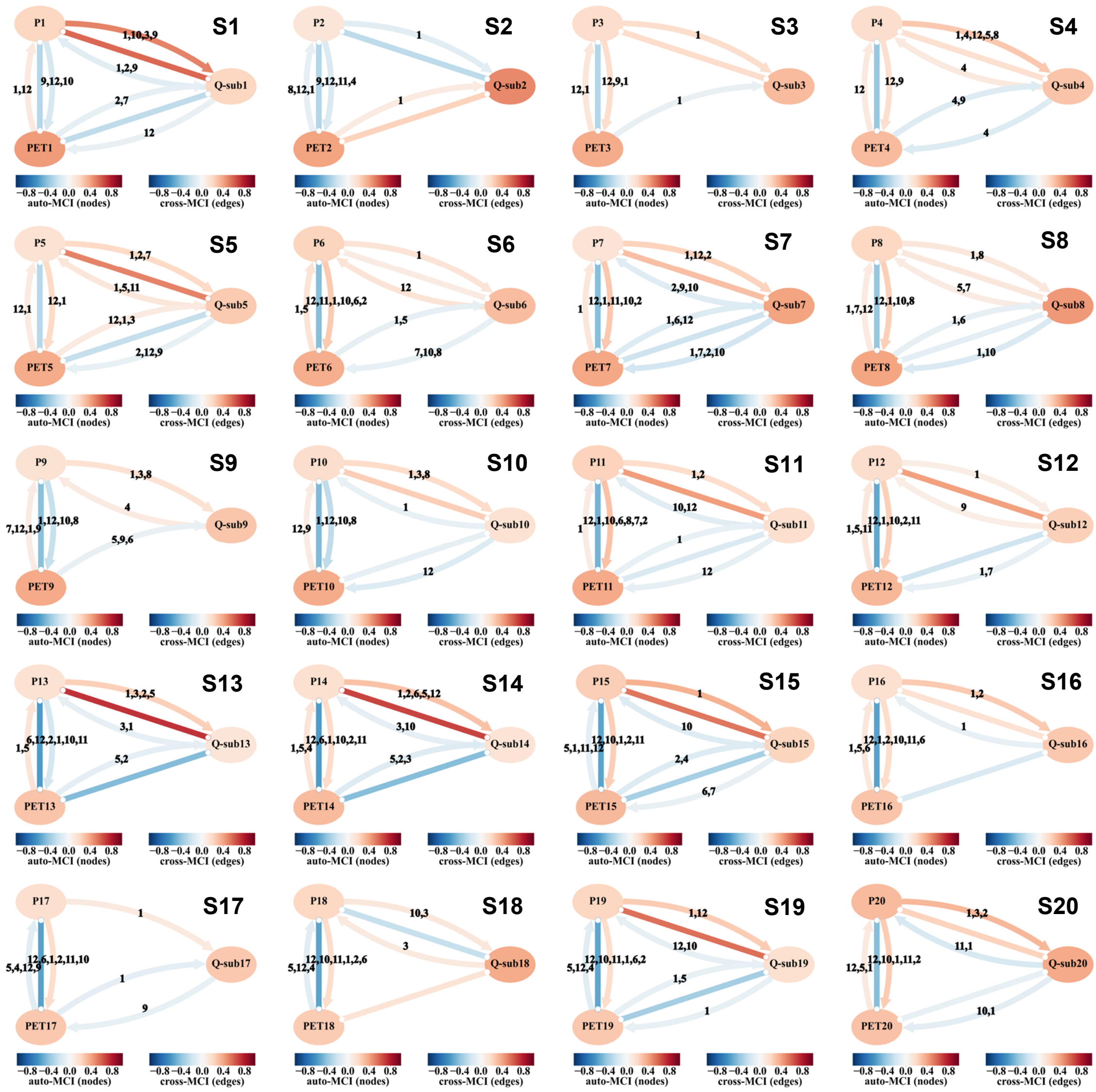

Supplementary Fig. 18: The significant causal network among monthly runoff contributions (Q_{sub}), precipitation (*P*), and potential evapotranspiration (*PET*) across sub-catchments from 1952 to 2021, obtained through PCMCI+ analysis (significance level = 0.05, maximum time lag = 12 months). Node colors represent auto-correlation strength, while link edge colors indicate the (positive or negative) MCI coefficient strength between variables. Arrow direction and labels denote the causal relationship between time-lagged data of the source variable (with lag time in months indicated by link labels) and contemporaneous data of the target variable.

Supplementary Tables

Supplementary Table 1. Land use reclassification and meaning of each land use type.

ID	Name		Meaning	Degree of human activities
1	Arable land		Refers to land used for crop cultivation, including paddy fields and dry land.	Relatively larger
2	Forest land		Refers to land used for forestry, including areas with trees, shrubs, bamboo, and coastal mangroves.	Relatively smaller
3	Grassland		Refers to all types of grasslands dominated by herbaceous plants with a coverage of over 5%, including shrub grasslands primarily used for grazing and open forest grasslands with a canopy density of less than 10%.	Relatively smaller
4	Construction land		Refers to the land used by urban and rural residents, as well as land for industry, mining, transportation, and other purposes outside these areas.	Relatively larger
5	Other land		Currently unused land, including lands that are difficult to utilize. Examples include sandy land, bare land, and saline-alkali land.	Relatively smaller
6	Water area	Rivers and canals	Refers to naturally formed or artificially excavated rivers and lands below the perennial water level of the main riverbed.	Relatively larger
7		Lakes	Refers to land below the perennial water level of naturally formed water accumulation areas.	Relatively smaller
8		Reservoirs and ponds	Refers to land below the perennial water level of artificially constructed water storage areas.	Relatively larger
9		Permanent ice and snow	Refers to lands that are perennially covered by glaciers and snow.	Relatively smaller
10		Beaches	Refers to the land between the water level of rivers and lakes during the normal period and the water level during the flood period.	Relatively smaller

Supplementary Table 2. Location information of 20 hydrological stations, the catchment area from each site's historical records and re-conducted hydrological analysis extraction, as well as their relative errors, and the sub-catchment areas reclassified based on each hydrological station.

ID	Hydrological station	River	Longitude (E)	Latitude (N)	Recorded area (km^2)	Analyzed area (km^2)	Relative error (%)	Sub-catchment	
								Name	Area (km^2)
1	Tangnaihai (TNH)	Yellow river	100.15	35.50	121,972	120,317	1.36	S1	120,317
2	Guide (GD)	Yellow river	101.40	36.03	133,650	131,497	1.61	S2	11,180
3	Xunhua (XH)	Yellow river	102.50	35.83	145,459	143,123	1.61	S3	11,626
4	Xiaochuan (XC)	Yellow river	103.33	35.93	181,770	178,964	1.54	S4	35,841
5	Lanzhou (LZ)	Yellow river	103.82	36.06	222,551	219,962	1.16	S5	40,998
6	Xiaheyan (XHY)	Yellow river	105.05	37.45	254,142	251,802	0.92	S6	31,840
7	Shizuishan (SZS)	Yellow river	106.79	39.25	309,146	307,043	0.68	S7	55,241
8	Sanhuhekou (SHHK)	Yellow river	108.78	40.61	347,909	347,120	0.23	S8	40,077
9	Toudaoguai (TDG)	Yellow river	111.06	40.27	367,898	367,740	0.04	S9	20,620
10	Fugu (FG)	Yellow river	111.08	39.04	404,039	404,561	0.13	S10	36,821
11	Wubao (WB)	Yellow river	110.72	37.45	433,514	435,176	0.38	S11	30,615
12	Longmen (LM)	Yellow river	110.58	35.67	497,552	498,236	0.14	S12	63,060
13	Hejin (HJ)	Fenhe river	110.80	35.57	38,728	39,226	1.29	S13	39,226
14	Xianyang (XY)	Weihe river	108.70	34.32	46,827	47,154	0.70	S14	47,154
15	Huaxian (HX)	Weihe river	109.76	34.58	106,498	106,228	0.25	S15	59,074
16	Tongguan (TG)	Yellow river	110.33	34.60	682,141	682,173	< 0.01	S16	38,483
17	Sanmenxia (SMX)	Yellow river	111.37	34.82	688,421	688,270	0.02	S17	6,097

ID	Hydrological station	River	Longitude (E)	Latitude (N)	Recorded area (km^2)	Analyzed area (km^2)	Relative error (%)	Sub-catchment	
								Name	Area (km^2)
18	Xiaolangdi (XLD)	Yellow river	112.41	34.92	694,221	694,132	0.01	S18	5,862
19	Huayuankou (HYK)	Yellow river	113.67	34.91	730,036	729,598	0.06	S19	35,466
20	Lijin (LJ)	Yellow river	118.30	37.52	751,869	751,869	0	S20	22,271

Supplementary Table 3. The key human activity factors causing runoff changes in each sub-catchment from Period 1 (1952-1969) to Period 2 (1970-1986).

Sub-catchment	Runoff contribution of sub-catchment $m^3\ s^{-1}$	Proportion of runoff change attributed to climate change	Proportion of runoff change attributed to human activities	Key human activity factors
S1	67.52	0.58	0.42	Melting of snow and ice
S2	-18.64	0.05	-1.05	Water storage in reservoirs
S3	-37.46	0.04	-1.04	Expansion of forest lands, farmlands, and construction lands
S4	10.00	0.21	0.79	Conversion of farmland to forest land
S5	-28.86	0.09	-1.09	Increase in farmland
S6	-3.70	-0.28	-0.72	Increase in farmland
S7	-12.84	-0.24	-0.76	Increase in construction land
S8	3.06	-0.04	1.04	Significant increase in farmland, but substantial decrease in water area
S9	-14.90	-0.05	-0.95	Increase in farmland
S10	-25.45	-0.27	-0.73	Increase in farmland
S11	-25.16	-0.53	-0.47	Significant decrease in farmland, but increase in water area and construction land
S12	-29.78	-0.81	-0.19	Increase in farmland, possibly with other water sources
S13	-29.44	-0.12	-0.88	Increase in farmland, possibly with other water sources
S14	-57.64	-0.83	-0.17	Decrease in farmland, but increase in

Sub-catchment	Runoff contribution of sub-catchment $m^3\ s^{-1}$	Proportion of runoff change attributed to climate change	Proportion of runoff change attributed to human activities	Key human activity factors
				reservoir water storage and construction land
S15	-17.08	-0.67	-0.33	Increase in farmland, but decrease in forest land and water area
S16	8.35	-1.42	2.42	Increase in farmland, but decrease in forest land, construction land, and water area
S17	-10.29	-0.12	-0.88	Decrease in farmland, but significant increase in construction land
S18	-22.53	-0.08	-0.92	Decrease in farmland and construction land, but increase in forest land and reservoir area
S19	-41.54	-0.26	-0.74	Increase in farmland
S20	-251.82	-0.04	-0.96	Increase in farmland

Note: Positive values indicate a positive contribution, while negative values indicate a negative contribution.

Supplementary Table 4. The key human activity factors causing runoff changes in each sub-catchment from Period 2 (1970-1986) to Period 3 (1987-2003).

Sub-catchment	Runoff contribution of sub-catchment $m^3\ s^{-1}$	Proportion of runoff change attributed to climate change	Proportion of runoff change attributed to human activities	Key human activity factors
S1	-145.64	-0.14	-0.86	Increase in farmland, decrease in water from melting snow and ice
S2	-22.71	0	-1	Expansion of farmland area with water storage in reservoirs
S3	2.84	-0.83	1.83	Decrease in farmland
S4	-71.98	-0.23	-0.77	Significant increase in farmland and construction land
S5	3.92	0.31	0.69	Decrease in farmland with some water from melting snow and ice
S6	-30.60	-0.05	-0.95	Decrease in farmland
S7	-0.35	-0.58	-0.42	Increase in farmland, decrease in water area
S8	-24.77	-0.01	-0.99	Conversion of farmland to forest, but increase in construction land
S9	-0.76	-0.38	-0.62	Conversion of farmland to forest, but increase in construction land
S10	-9.47	-0.18	-0.82	Conversion of farmland to forest, but increase in construction land and water area
S11	-12.81	-0.25	-0.75	Conversion of farmland to forest, but increase in construction land
S12	5.57	-1.57	2.57	Conversion of farmland to forest
S13	-12.13	-0.44	-0.56	Significant decrease in farmland, but increase

Sub-catchment	Runoff contribution of sub-catchment m^3 s^{-1}	Proportion of runoff change attributed to climate change	Proportion of runoff change attributed to human activities	Key human activity factors
				in construction land area
S14	-54.12	-1.37	0.37	Significant decrease in farmland, but increase in construction land area
S15	-12.21	-0.89	-0.11	Significant decrease in farmland, but increase in construction land area
S16	-19.10	-0.48	-0.52	Conversion of farmland to forest, increase in construction land, decrease in water area
S17	-28.24	-0.09	-0.91	Increase in farmland
S18	-11.92	-0.22	-0.78	Decrease in farmland, but significant water storage in reservoirs
S19	-29.89	-0.48	-0.52	Decrease in farmland, but increase in construction land area
S20	-111.96	-0.03	-0.97	Significant increase in construction land area, increase in farmland and reservoir area, but decrease in water area

Note: Positive values indicate a positive contribution, while negative values indicate a negative contribution.

Supplementary Table 5. The key human activity factors causing runoff changes in each sub-catchment from Period 3 (1987-2003) to Period 4 (2004-2021).

Sub-catchment	Runoff contribution of sub-catchment m^3 s^{-1}	Proportion of runoff change attributed to climate change	Proportion of runoff change attributed to human activities	Key human activity factors
S1	122.50	1.03	-0.03	Increase in farmland and construction land
S2	-11.52	0.64	-1.64	Increase in farmland, construction land, and reservoir area
S3	26.97	0.34	0.66	Significant decrease in farmland
S4	29.22	1.02	-0.02	Significant decrease in farmland, but significant increase in construction land
S5	46.46	0.44	0.56	Significant decrease in farmland, increase in construction land
S6	-4.01	0.4	-1.4	Decrease in farmland, significant increase in construction land
S7	-38.62	0	-1	Significant increase in farmland and construction land
S8	-0.50	0.57	-1.57	Significant increase in farmland and construction land
S9	-14.87	0.03	-1.03	Decrease in farmland, but significant increase in construction land
S10	-6.66	0.02	-1.02	Decrease in farmland, but significant increase in construction land
S11	-2.37	2.43	-3.43	Significant increase in construction land
S12	-58.04	0.24	-1.24	Significant increase in construction land
S13	5.17	0.91	0.09	Significant increase in construction land

Sub-catchment	Runoff contribution of sub-catchment m^3 s^{-1}	Proportion of runoff change attributed to climate change	Proportion of runoff change attributed to human activities	Key human activity factors
S14	25.74	2.88	-1.88	Significant decrease in farmland, but significant increase in construction land
S15	5.62	2.36	-1.36	Significant decrease in farmland, but significant increase in construction land
S16	-30.53	0.36	-1.36	Significant decrease in farmland, but significant increase in construction land
S17	14.20	0.13	0.87	Significant decrease in farmland, but significant increase in construction land
S18	51.08	0.05	0.95	Significant decrease in farmland and forest land, significant increase in construction land
S19	-1.29	9.49	-10.49	Significant decrease in farmland, but significant increase in construction land
S20	94.40	0.17	0.83	Significant decrease in farmland, but significant increase in construction land

Note: Positive values indicate a positive contribution, while negative values indicate a negative contribution.

Supplementary References:

1. Xie, P., Gu, H., Sang, Y. F., Wu, Z. & Singh, V. P. Comparison of different methods for detecting change points in hydroclimatic time series. *Journal of Hydrology* **577**, doi:10.1016/j.jhydrol.2019.123973 (2019).
2. Dey, P. & Mishra, A. Separating the impacts of climate change and human activities on streamflow: A review of methodologies and critical assumptions. *Journal of Hydrology* **548**, 278-290, doi:10.1016/j.jhydrol.2017.03.014 (2017).
3. Luan, J. et al. Evaluating the uncertainty of eight approaches for separating the impacts of climate change and human activities on streamflow. *Journal of Hydrology* **601**, doi:10.1016/j.jhydrol.2021.126605 (2021).
4. Wang, W., Zhang, Y. & Tang, Q. Impact assessment of climate change and human activities on streamflow signatures in the Yellow River Basin using the Budyko hypothesis and derived differential equation. *Journal of Hydrology* **591**, doi:10.1016/j.jhydrol.2020.125460 (2020).